

High Resolution Radar Imaging of Moving Humans Using Doppler Processing and Compressed Sensing

Shobha Sundar Ram, *Member, IEEE*, and Angshul Majumdar, *Member, IEEE*

Abstract—Frontal radar imaging of human activities may be useful in certain applications, such as through-wall surveillance, where cameras and x-ray sensors cannot be deployed. High resolution radar images are currently obtained using electrically large antenna apertures operating at high frequencies. But high frequencies are heavily attenuated by most walls. Also, the implementation of a radar with lots of array elements and associated data acquisition channels is costly and complex. In this paper, we propose methods to generate high-resolution Doppler-enhanced radar images of moving humans at low carrier frequencies with limited number of antenna elements. When a human moves, different body parts give rise to distinct Doppler returns. The key feature of our method is to dynamically resolve multiple body parts of the human across three dimensions: Doppler, azimuth and elevation. The additional Doppler dimension allows us to relax the resolution requirements in terms of the carrier frequency and number of array elements across the other dimensions. We further reduce the number of array elements below the Nyquist limits by incorporating compressed sensing principles into two dimensional beamforming since compressed sensing is particularly suited for solving certain types of under resolved problems. We test our technique on simulated electromagnetic radar scattered data from a moving human for different radar configurations. We also study the robustness of the proposed technique to noise.

Index Terms—High-resolution imaging, radar imaging, Doppler radar, compressed sensing, micro-Doppler.

I. INTRODUCTION

Radars are uniquely suited for sensing humans for law enforcement, security and surveillance operations, biomedical studies and sports. Both narrowband and ultra wideband (UWB) radars have been investigated and developed for detecting and tracking humans in non-line-of-sight conditions where cameras and x-ray sensors cannot be deployed [1]–[5]. UWB radars provide high range resolution profiles of humans while Doppler radars provide microDoppler information regarding different human activities [6]. However, untrained radar operators may find both of these signatures difficult to interpret. This limitation can be partially overcome with the assistance of sophisticated target recognition algorithms based on supervised learning techniques [7]–[12]. Such algorithms involve the challenges of generating large training databases under a variety of operating conditions. Another approach would be to directly generate frontal radar images of humans since frontal views convey more information regarding different human activities than top views. Radar images, however unlike optic images, are of very low resolution since they are limited by the carrier frequency and the size of the radar aperture.

Most walls heavily attenuate high frequency radar signals. Also, electrically large apertures comprising lots of array elements are required to obtain high resolution [13]. Such a radar system with multiple antenna elements each with an associated data acquisition channel is both costly and complex to implement. Synthetic aperture (SAR) techniques are also not suitable for realizing such large apertures since human motions may significantly degrade SAR images. In this paper, we propose using a combination of Doppler processing with compressed sensing based array processing to image moving humans. Doppler processing allows us to reduce the carrier frequency while compressed sensing enables two-dimensional beamforming with limited number of array elements.

Continuous wave Doppler radars are inherently suitable for imaging moving humans for multiple reasons. First, stationary background clutter is suppressed while using continuous wave signals. Second, Doppler signals are far more robust to multipath caused by walls and floors than UWB waveforms [14]. Finally, since humans are non-rigid moving targets, the movements of different body parts give rise to distinct microDopplers [6]. Lin, in [15], exploited the last property towards imaging humans using a three-element Doppler radar. The different body parts were first resolved on the basis of their Dopplers. Then the azimuth and elevation position of each body part with a distinct Doppler was estimated using two-dimensional interferometry. This low cost solution is effective only when the Dopplers of the different body parts are sufficiently well resolved. In our paper, we combine Doppler processing with two-dimensional array processing to dynamically resolve the different scatterers on the human body in three dimensions based on their distinct Dopplers, azimuth and elevation positions.

The resolution in the azimuth-elevation plane or front-view of a spatially large radar target such as a human is limited by the size of the two-dimensional array aperture. The number of array elements becomes very large if the elements are closely spaced to allow for beam scanning. Compressed sensing (CS) is a signal processing technique where the number of measurements required to recover an image (or any signal) can be reduced below the Nyquist limits if the image is inherently compressible in some domain [16], [17]. CS has been successfully applied in several image processing and magnetic resonance imaging applications [18], [19]. More recently, the radar community has applied CS for reducing the data acquisition bandwidths associated with synthetic aperture and inverse synthetic aperture radar applications [20]–[33]. In [34], CS was used for imaging targets behind walls using wideband signals. CS has also been used for reducing the

number of sensors in a multiple input multiple output (MIMO) radar system [35], [36]. In this paper, we will introduce CS to two-dimensional array processing to generate frontal images of humans. CS enables us to reduce the number of array elements below the Nyquist limits though the size of the aperture remains the same.

In section II, we present the simulation model of the electromagnetic scattering from moving humans on a Doppler radar system. We also study the limitations of directly imaging humans using two-dimensional array processing. In section III, we integrate CS principles with array processing to reduce the number of array elements required to recover the radar image. We also examine noise effects on the image reconstruction capabilities of the algorithm. In section IV, we combine Doppler processing with array processing to image humans at low carrier frequencies. Finally in section V, we combine Doppler processing and CS based beamforming to generate high resolution images of a moving human. We carry out noise analysis to test the robustness of the proposed algorithm.

II. SIMULATION OF TWO-DIMENSIONAL BEAMFORMING

We simulate Doppler radar data from moving humans by combining computer animation data, derived from motion capture technology, with electromagnetic primitive based modeling of human body parts [14]. We consider a realistic motion where a human spreads his arms wide at a distance of 10m, along the X axis, before a continuous wave radar. The human is 1.5m tall (head to foot), along the Y axis, and 1.5m wide (right to left hand) along the Z axis. The arms, legs, torso and head are modeled as primitives such as spheres and ellipsoids. The human is therefore a complex target with multiple point scatterers corresponding to the phase centers of these primitives. We model the radar with a two-dimensional uniform planar transceiver array with $[N \times N]$ elements spaced half-wavelength apart in both dimensions as shown in Fig.1. The array is placed in the YZ plane with the central element located at $[0, 1, 1]m$. The antenna elements are isotropic. The simulation model enables the parametrization of the radar carrier frequency, the number of elements in the array and the sampling frequency of the data acquisition system. We generate the front view radar image of the human at each time instant, $X_{\theta,\phi}(t)$, from the instantaneous $[N \times N]$ measurement vector at the transceiver array, $Y(t)$, using the inverse of

$$Y(t) = FX_{\theta,\phi}(t) \quad (1)$$

where F is the two-dimensional Fourier transform or the beamforming function. The image is a function of spherical coordinates, azimuth (ϕ) and elevation (θ).

A. Results and Inferences

First, we consider a case where the carrier frequency is set at 30GHz and the antenna array with $[80 \times 80]$ elements. The choice of the carrier frequency is dictated by a tradeoff between two factors. One, higher the carrier frequency, greater is the resolution of the image. Also the far-field radius of the radar reduces; Second, high carrier frequencies are unsuitable for through-wall purposes. Also, high frequency

radars are usually more expensive. Therefore, we have selected the lowest carrier frequency that would generate an image with desired resolution characteristics. The antenna aperture is $[40cm \times 40cm]$ when the elements are spaced half-wavelength apart. The choice of radar parameters (carrier frequency, number of elements and size of aperture) are dictated by a tradeoff between the desired resolution characteristics in the radar image and the cost and complexity of the radar. This is illustrated in the following three cases. Fig.2(a) shows the front view radar image of the human. The figure has not been reformatted to Cartesian coordinates. We can identify the head, torso, arms and legs of the human even though the resolution is poor compared to an optic image. Note that the human is not in the far-field region of the radar even with the high carrier frequency. Next, the number of elements in each dimension is reduced by a factor of 4 i.e. the transceiver is set with a $[20 \times 20]$ array while the spacing between the elements remains the same. Therefore, the aperture size is $[10cm \times 10cm]$. Fig.2(b) shows the front view image of the human at the same time instant as the previous case. The reduction in the size of the aperture (and the number of elements) has severely degraded the quality of the image due to reduced resolution. Next we reduce the carrier frequency to 7.5GHz while the antenna array is modified to an $[80 \times 80]$ array of $[160cm \times 160cm]$ size. The front-view image is shown in Fig 2(c). Despite the increase in aperture size, the reduction of the carrier frequency by a factor of 4 has severely degraded the image. This is because two dimensional array processing through Fourier transform is ideally meant only for far field data. Near field distortions become dominant at lower carrier frequencies. The results show that the resolution of the image is a function of both the carrier frequency and the number of antenna elements. A radar operating at a high frequency with large number of antenna elements, each with an associated data acquisition channel, would be costly to build and ineffective in through-wall scenarios. Therefore, we examine methods to reduce both the frequency and the number of elements in the following sections.

III. ARRAY PROCESSING WITH COMPRESSED SENSING

In this section, we briefly describe how compressed sensing (CS) principles can be used for realizing high resolution radar images of human activities with a subset of elements from an $[N \times N]$ array. Preliminary studies of imaging spatially large targets with CS based array processing were presented in [37]. Our objective is to solve the inverse problem defined in (1). The problem becomes an under-determined set of equations when the number of array elements is below the resolution requirements of the image to be captured. If the choice of the subset of elements is random while the size of the aperture remains the same, then F in (1) can be modified to RF where R is a random matrix of size $[N \times N]$ with values of either 1's or 0's. This implies that measurements are taken at a random subset of the elements of the antenna array. CS is especially suited for solving under-determined problems provided two conditions are satisfied:

- 1) the image that is to be reconstructed is sparse in some basis;

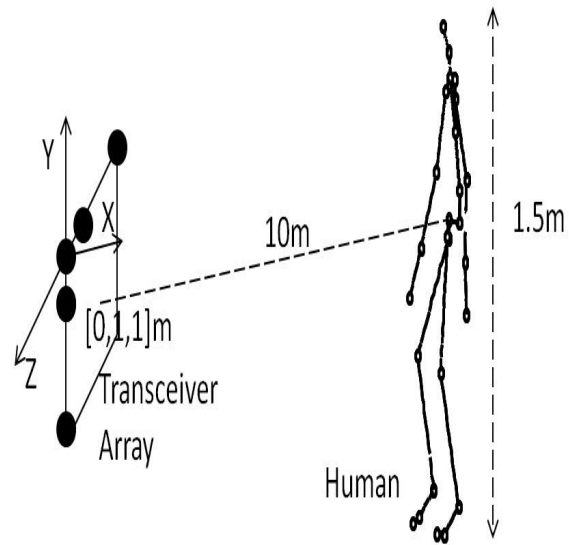


Fig. 1. Simulation model of moving human before a Doppler radar with two-dimensional uniform planar array

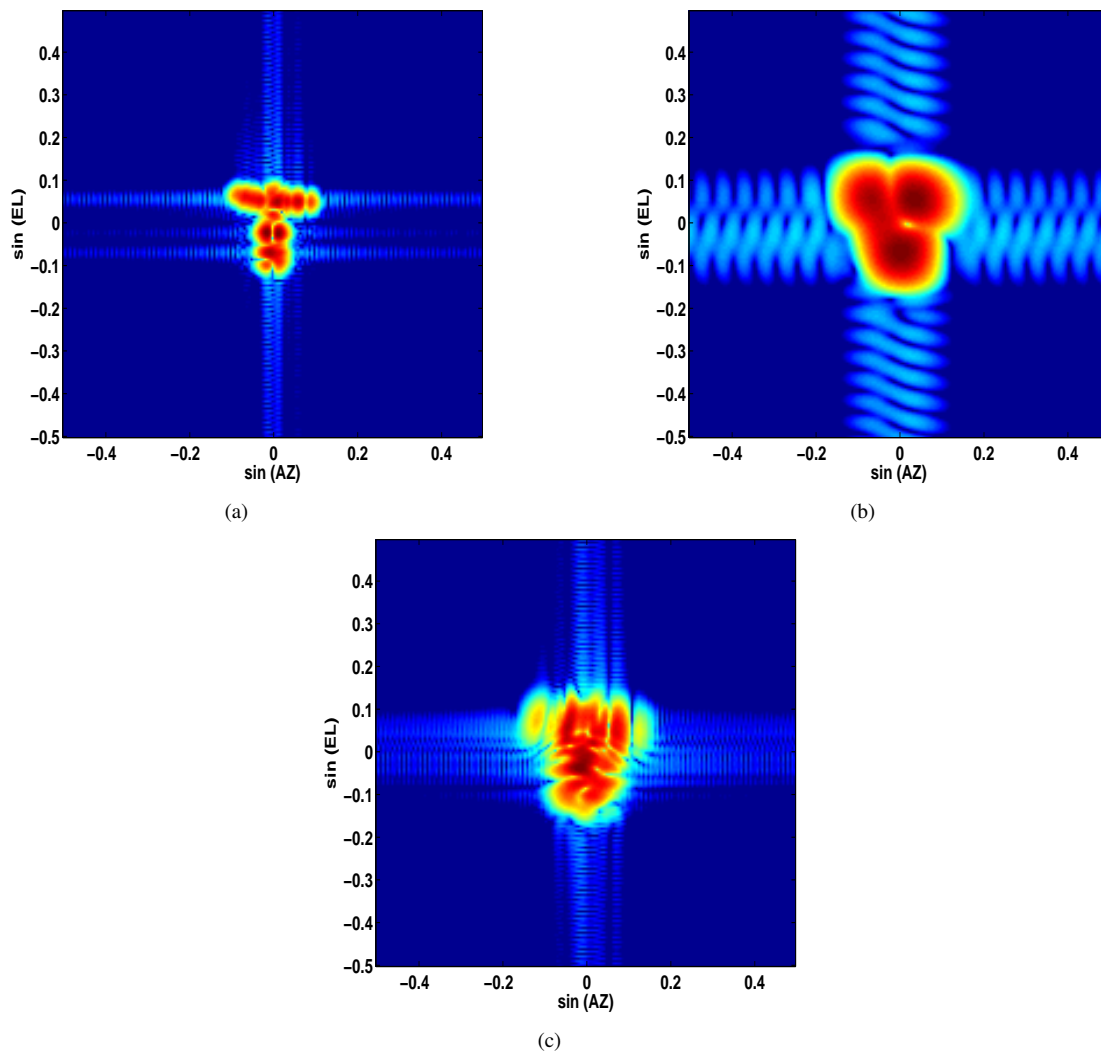


Fig. 2. Frontal radar image of a human captured by (a) $[80 \times 80]$ array configuration operating at 30GHz; (b) $[20 \times 20]$ array configuration operating at 30GHz; (c) $[80 \times 80]$ array configuration operating at 7.5GHz

2) the measurement basis (in this case random Fourier) must be incoherent with respect to the sparsifying basis. We represent the image recovered from CS, $X_{\theta,\phi}^c$, for each frame as (2)

$$\alpha(t) = \psi X_{\theta,\phi}^c(t) \quad (2)$$

where ψ is the Dirac/ identity basis that transforms $X_{\theta,\phi}^c(t)$ to $\alpha(t)$. The choice of Dirac as the sparsifying basis is suitable for our problem since the incoherence between Dirac and the Fourier basis is maximum for all possible pairs of bases. Second, the radar image is quite sparse in the Dirac spatial basis as shown in Fig.2(a). Thus, the measurement vector at any time instant can be represented as

$$Y(t) = RF\psi^{-1}\alpha(t) \quad (3)$$

Since α is sparse, we solve (3) for α using l_1 minimization techniques described in [38]. Finally the image, $X_{\theta,\phi}^c$, is reconstructed from the inverse of (2).

A. Results and Inferences

We choose a random 50% subset (3200 elements) of the total number of elements of an $[80 \times 80]$ array operating at 30GHz. Using CS based array processing, the radar image is recovered and presented in Fig.3(a). When we compare this figure with Fig.2(a), we observe that the quality of the image is retained despite the 50% reduction in the number of array elements. Fig.3(b) shows the radar image obtained when we use a random 10% subset (640 elements) of the total number of elements of the $[80 \times 80]$ array. Here, we observe image recovery errors in the form of a noisy background.

We quantitatively studied the effectiveness of CS for three uniform planar array configurations consisting of $[80 \times 80]$ elements, $[20 \times 20]$ elements and $[5 \times 5]$ elements. All three configurations operate at 30GHz and the elements are spaced half-wavelength apart. Fig.4(a) shows the normalized mean square error (NMSE) of image reconstruction as a function of the degree of compression of the number of elements of the arrays. The normalized mean square error for each frame is defined by

$$NMSE(\%) = \frac{|X_{\theta,\phi}^c(t) - X_{\theta,\phi}(t)|^2}{|X_{\theta,\phi}^c(t)|^2} \times 100 \quad (4)$$

Here $X_{\theta,\phi}$ is the image recovered using array processing with all the elements in the antenna array as described in (1). $X_{\theta,\phi}^c$ is the image recovered using reduced number (CS %) of elements as described in (3). The error is computed and averaged over 50 frames and shown in Fig.4(a). We observe that the reconstruction error increases for all three cases as we reduce the number of elements (or increase the compression). We also observe that for the same degree of compression, the error is much lower for the $[80 \times 80]$ array followed by the $[20 \times 20]$ and $[5 \times 5]$ arrays. Therefore, we conclude that the effectiveness of CS solutions deteriorate for small array sizes.

Next, we study the robustness of CS based array processing to noise. Additive white Gaussian noise is added to the measurement data $Y(t)$ and the normalized mean square error is computed for an $[80 \times 80]$ radar system operating at 30GHz.

The normalized mean square error for each frame is defined by

$$NMSE(\%) = \frac{|X_{\theta,\phi}^{nc}(t) - X_{\theta,\phi}^c(t)|^2}{|X_{\theta,\phi}^c(t)|^2} \times 100 \quad (5)$$

where $X_{\theta,\phi}^{nc}$ is the image recovered from noisy measurements for the same degree of compression utilized for retrieving $X_{\theta,\phi}^c$ from noiseless measurement data. Fig. 4(b) shows the NMSE as a function of the degree of compression for three signal-to-noise ratios (SNR). We observe that the error increases with higher noise levels. However, the overall performance of the algorithm is robust to noise (error below 25%) and deteriorates only when the SNR is 10dB or worse.

In all of these results, the range of the target with respect to the radar is fixed. However, if the target's range with respect to the radar increases, the two-dimensional beamforming will become increasing linear and we can expect less distortions due to near field effects. However, the actual size of the image with respect to the aperture will reduce. This will have two consequences: One, the resolution requirements will increase which implies we will need larger radar apertures; Two, the sparsity of the image in the radar aperture will increase which lends itself to further compression of the number of antenna elements.

IV. JOINT DOPPLER AND ARRAY PROCESSING

Humans are non-rigid targets that rarely remain still. Different body parts of the humans give rise to distinct microDoppler components which are best represented in the joint time-frequency space through the short time Fourier transform (STFT) [6], [39]. This is shown in

$$\chi(f, t) = \int Y(\tau)h(t - \tau)e^{-j2\pi f\tau}d\tau \quad (6)$$

Here, $\chi(f, t)$ is a vector of size $[N \times N]$ that consists of the joint time-frequency representation of the measured data at the array and $h(t)$ is a moving time window with fixed width. Array processing or two dimensional beamforming is carried out for each Doppler frequency, as shown in

$$W_{\theta,\phi}(f, t) = F^{-1}\chi(f, t) \quad (7)$$

Therefore, the measurement data have been effectively resolved in three dimensions: Doppler (f), elevation and azimuth for each time interval. The radar image of the human for time t is realized from the coherent sum of point spread responses from the peak scatterers, W_{θ^m, ϕ^m}^m , for each Doppler.

$$X_{\theta,\phi}^d(t) = \sum_f W_{\theta^m, \phi^m}^m(f, t)H(\theta - \theta^m, \phi - \phi^m) \quad (8)$$

We choose a high resolution point spread function, $H(\theta, \phi)$, in the two dimension space centered at the positions (θ^m, ϕ^m) corresponding to the peak scatterer for each Doppler frequency. Note that $X_{\theta,\phi}^d(t)$, derived from (8), is different from the image, $X_{\theta,\phi}(t)$, derived from (1), in the following ways.

- 1) Imaging using combined Doppler processing and two-dimensional beamforming is effective only when carried out on targets with significant radial velocity components. There may be some complex motions where all the different body parts of the human may not move.

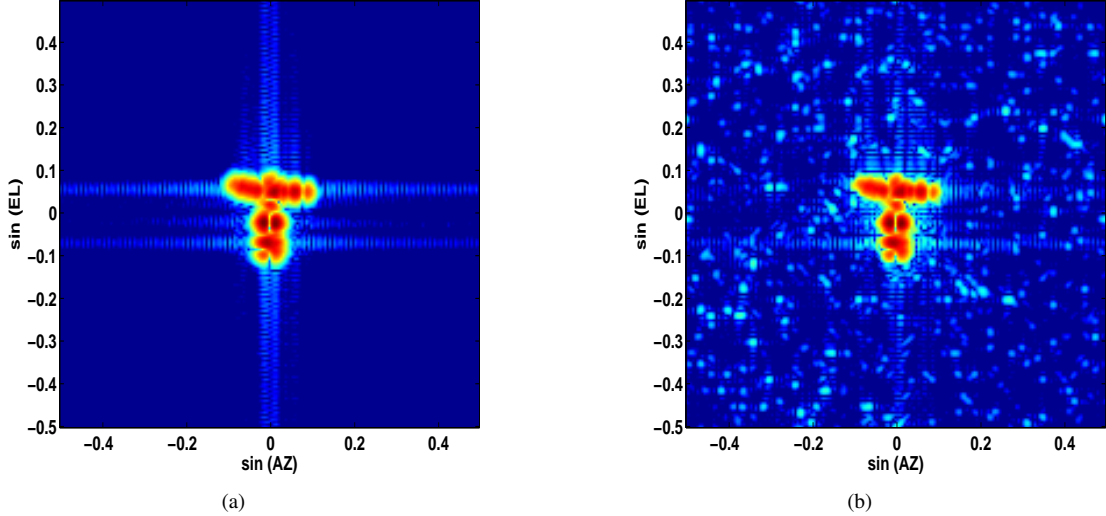


Fig. 3. Frontal radar image of a human captured by combined compressed sensing and array processing using (a) 50% of sensors; (b) 10% of sensors of an $[80 \times 80]$ array configuration operating at 30GHz

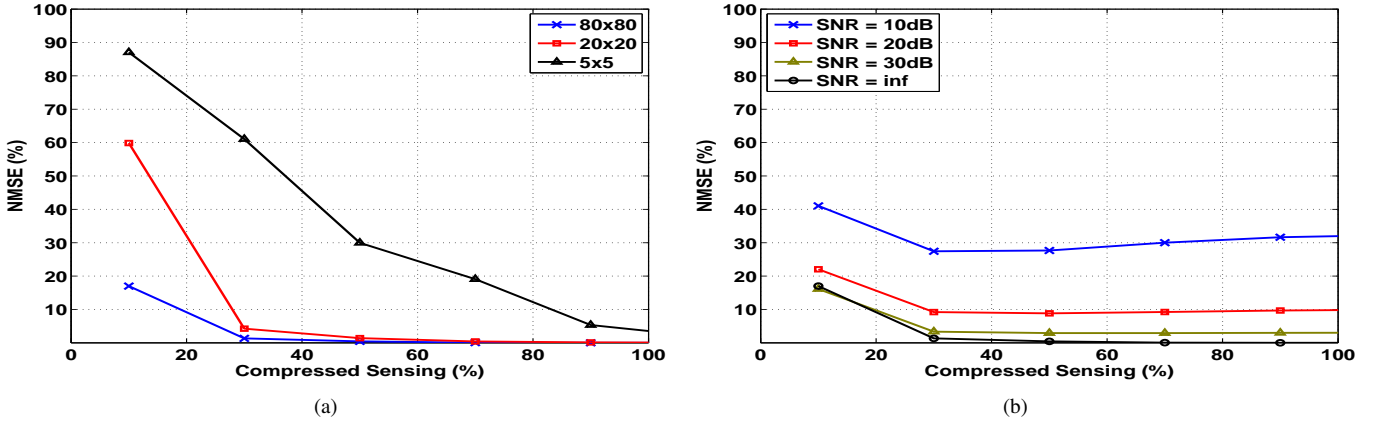


Fig. 4. Normalized mean square error of image recovery while using compressed sensing with array processing versus degree of compression, as a function of (a) $[N \times N]$ size of the array configuration; (b) signal to noise ratio of the radar system

For example, when a human is standing still but waving his hand. In those cases, Doppler based imaging will be restricted only to those body parts that are moving. Likewise, the Dopplers are maximum when the motions are radial with respect to the radar.

- 2) Since the point scatterers on the complex human target are resolved across three dimensions in (8) rather than two dimensions as in (1), the resolution criteria for imaging in terms of the number of array elements and the carrier frequency of the radar may be relaxed.
- 3) The positions and velocities of the body parts of the human may not be fixed during the entire dwell time of the STFT. This may result in some blurring of the image.
- 4) There may be significant overlap in the microDopplers of the different body parts during some time intervals which may result in the degradation of the quality of the images.

A. Results and Inferences

We test our algorithm on simulated radar scattered data from a human walking in a straight line from an initial stand off distance of 10m towards a Doppler radar for 3 seconds. The human motion is derived from motion capture data and hence is realistic. The average speed of the human is $1.4m/s$. This data is different from the data used in the previous two sections where the human motion had negligible radial motions and hence very low microDopplers. We consider a walking motion since this is perhaps one of the more common regularized motions undertaken by humans in indoor environments. Also, when a human walks, most body parts move at distinct radial velocities except for the head which moves at the same velocity as the torso. Hence we can, potentially, image the entire human body. The size of the human remains the same as the previous case discussed in Section.II-A. The radar consists of a uniform planar array of $[20 \times 20]$ elements operating at 7.5GHz where the elements are spaced half wavelength apart. The different scatterers on the body are first resolved along the Doppler dimension through the STFT using a moving

time window of $0.05s$ using (6). Next, the azimuth and elevation positions are determined for each Doppler using two-dimensional array processing (7). The peak scatterers for every Doppler are coherently added to generate the radar image shown in Fig.5(a). We are able to identify the arms, legs and the torso of the human. It is difficult to identify the head since there is considerable overlap between the microDoppler of the head and torso. The quality of the image is superior to Fig.2(b) and Fig.2(c). This implies, that we are able to successfully image the human despite significantly relaxing the resolution criteria. In other words, a good quality image is generated though the operating frequency and the number of array elements across each dimension have been reduced by a factor of 4. Note that these results are obtained when the human is walking normally towards the radar. If the human were to walk at an angle with respect to the radar, there is greater likelihood of overlap between the low micro-Dopplers and azimuth positions of body parts resulting in degradation in the image quality.

We compare this result with two other cases. In the first case, the array consists of $[5 \times 5]$ elements operating at $7.5GHz$ and the result is shown in Fig.5(b). The quality of the image has degraded due to the poor azimuth-elevation resolution caused by the smaller sized aperture. In the second case, the array consists of $[20 \times 20]$ elements operating at $1.875GHz$. Though the size of the aperture has increased, Fig.5(c) shows deterioration in imaging due to poor Doppler resolution of the multiple scatterers because of the low carrier frequency. These figures indicate the lower bounds on the performance with three dimensional Fourier processing. Therefore, we investigate alternate techniques for further reducing the number of array elements while retaining the carrier frequency at $7.5GHz$ in the next section.

V. JOINT DOPPLER PROCESSING AND COMPRESSED SENSING

In this section, we examine the possibility of combining Doppler processing, as described in the previous section, with compressed sensing based array processing to reduce the number of elements in the antenna array. We consider the measurement data at a random subset of a $[N \times N]$ antenna array. This is indicated by a vector masking function, R , on measurement vector Y . We perform Doppler processing on the time domain data at each element of this random subset as per (9).

$$\chi(f, t) = \int RY(\tau)h(t - \tau)e^{-j2\pi f\tau} d\tau \quad (9)$$

Then, we replace 2D Fourier processing with CS to generate $W_{\theta, \phi}^c$ for every Doppler from $\chi(f, t)$. This is based on the assumption that $W_{\theta, \phi}^c$ is sparse and compressible and can be represented by

$$\alpha(f, t) = \psi W_{\theta, \phi}^c(f, t) \quad (10)$$

where ψ is the Dirac basis which is incoherent with respect to the Fourier basis. Therefore,

$$\chi(f, t) = RF\psi^{-1}\alpha(f, t). \quad (11)$$

Then, l_1 minimization is carried out to solve (11) for the sparse transform α for each Doppler and $W_{\theta, \phi}^c$ is realized from the inverse of (10). Finally, the radar image, $X_{\theta, \phi}^{dc}$, is generated by the complex sum of the peak scatterers for each Doppler as detailed in (8). The CS steps used in this section are identical to those used in section III except that they are carried out on the frequency domain data rather than on time-domain data. The key feature of our algorithm is that CS has enabled us to recover the image using sub-Nyquist number of array elements i.e. to solve the under-resolved beamforming problem in the frequency domain.

A. Results and Inferences

We consider a $[20 \times 20]$ array that operates at $7.5GHz$ to image the moving human with the same simulation data used in Section IV. We perform joint Doppler processing and compressed sensing based array processing using a randomly chosen 50% subset of the total elements in the array. The Doppler processing is carried out over a dwell time of $0.05s$. Though the number of elements have reduced significantly, the size of the aperture remains that of a $[20 \times 20]$ array. The resulting image of the human over one time interval is shown in Fig.6(a). We observe that we can identify the arms, legs and torso of the human with 200 antenna elements. The process is repeated using 40 elements (10% subset of the antenna array) and the results are shown in Fig.6(b). Though the image shows slight degradation in quality, indicating that we may have reached the lower bounds of the performance of our proposed algorithm, we are still able to identify the different body parts. Fig.6(c) shows the image of the human using 25% of the elements of the $[20 \times 20]$ array when the signal to noise ratio level is 10dB. The image shows some noisy features though the human can still be distinguished.

In order to quantitatively study the impact of CS on different sizes of array configurations, we considered radar systems with $[20 \times 20]$, $[10 \times 10]$ and $[5 \times 5]$ antenna arrays. We computed the normalized mean square error (NMSE) of image reconstruction for each array configuration for different degrees of compression. In each case, we compared the recovered image with the corresponding image generated with Doppler and array processing of 100% of elements of the array. The error was averaged over a duration of $0.5s$ i.e. from 10 sets of data captured over a dwell time of $0.05s$ each. The results presented in Fig.7 show a higher overall level of error when compared to Fig.4(a) and Fig.4(b). This is due to the overlap of microDopplers of different body parts during some time intervals in the human walking motion and is a limitation associated with human Doppler data. Also, since the motion is realistic, the velocities of the body parts are not constant during the entire dwell time. This introduces blurring in some frames (not shown here). When the number of elements are reduced i.e. the degree of compression is increased, the image reconstruction error increases for all cases. Second, the error is highest for the $[5 \times 5]$ array followed by the $[10 \times 10]$ array and then the $[20 \times 20]$ array. For instance, the error is above 50% even when the degree of compression is low (90%) for the $[5 \times 5]$ array case. These results are consistent with the earlier results presented in Section III.

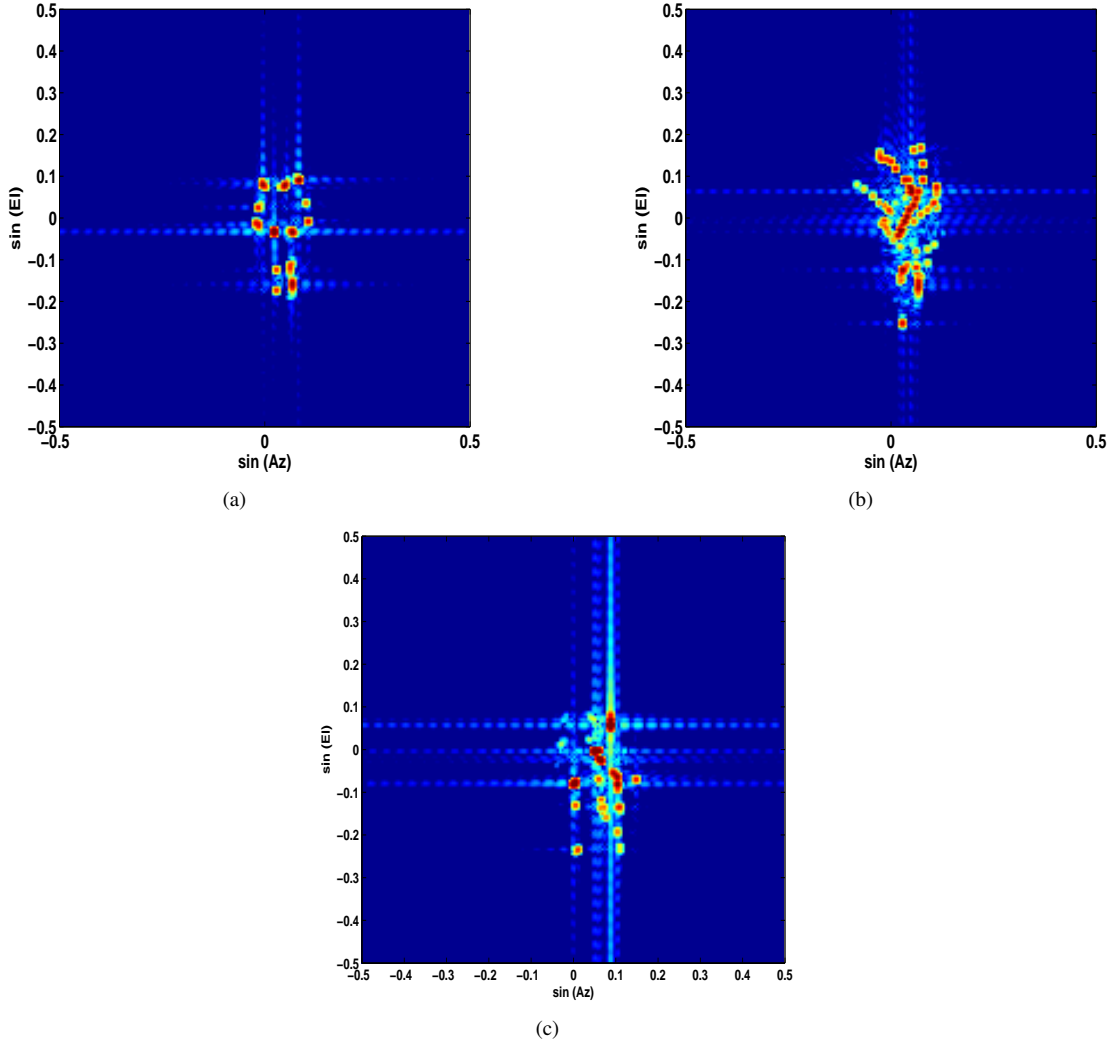


Fig. 5. Frontal radar image of a human captured by combined Doppler processing and array processing using (a) $[20 \times 20]$ array configuration at 7.5GHz; (b) $[5 \times 5]$ array configuration at 7.5GHz; (c) $[20 \times 20]$ array configuration at 1.875GHz

Next, we studied the quantitative impact of noise on CS for two cases: the $[20 \times 20]$ array data and the $[10 \times 10]$ array data. Noisy data were modeled by adding additive white Gaussian noise to the measurement data such that the signal to noise ratio is 10dB. The results in Fig.7 show that there is some deterioration in the image recovery due to noise. However, the actual size of the array is still a more significant factor towards determining the quality of the image reconstruction.

VI. CONCLUSION

Conventional radar implementations require electrically large antenna apertures with lots of array elements operating at high frequencies to generate high resolution images of spatially large moving targets such as humans. We have used Doppler processing with compressed sensing based array processing to overcome these two limitations. Different body parts are resolved based on their microDoppler, azimuth and elevation. By introducing an additional Doppler dimension, we are able to lower the radar carrier frequency and the number of array elements required to resolve the point scatterers across

the azimuth and elevation dimensions. Compressed sensing based beamforming enables us to further reduce the number of array elements below the Nyquist limits. We tested our methods on simulated radar data of a moving human for a wide variety of antenna array configurations. We were able to generate high quality radar images of a moving human at a stand off distance of 10m while reducing the carrier frequency from Ka band to C band and the number of array elements from 6400 to just 100 array elements. Our methods are fairly robust up to a signal to noise ratio level of 10dB. However, further investigation is required to estimate the robustness of the technique to clutter issues that may be introduced by multipath when the radar is operated in non-line-of-sight environments. Walls, for instance, may introduce attenuation, refraction, ringing and multipath to the radar signal which may impact the radar imaging methodology.

ACKNOWLEDGMENT

This work is supported by the DST Inspire Fellowship Award by the Government of India.

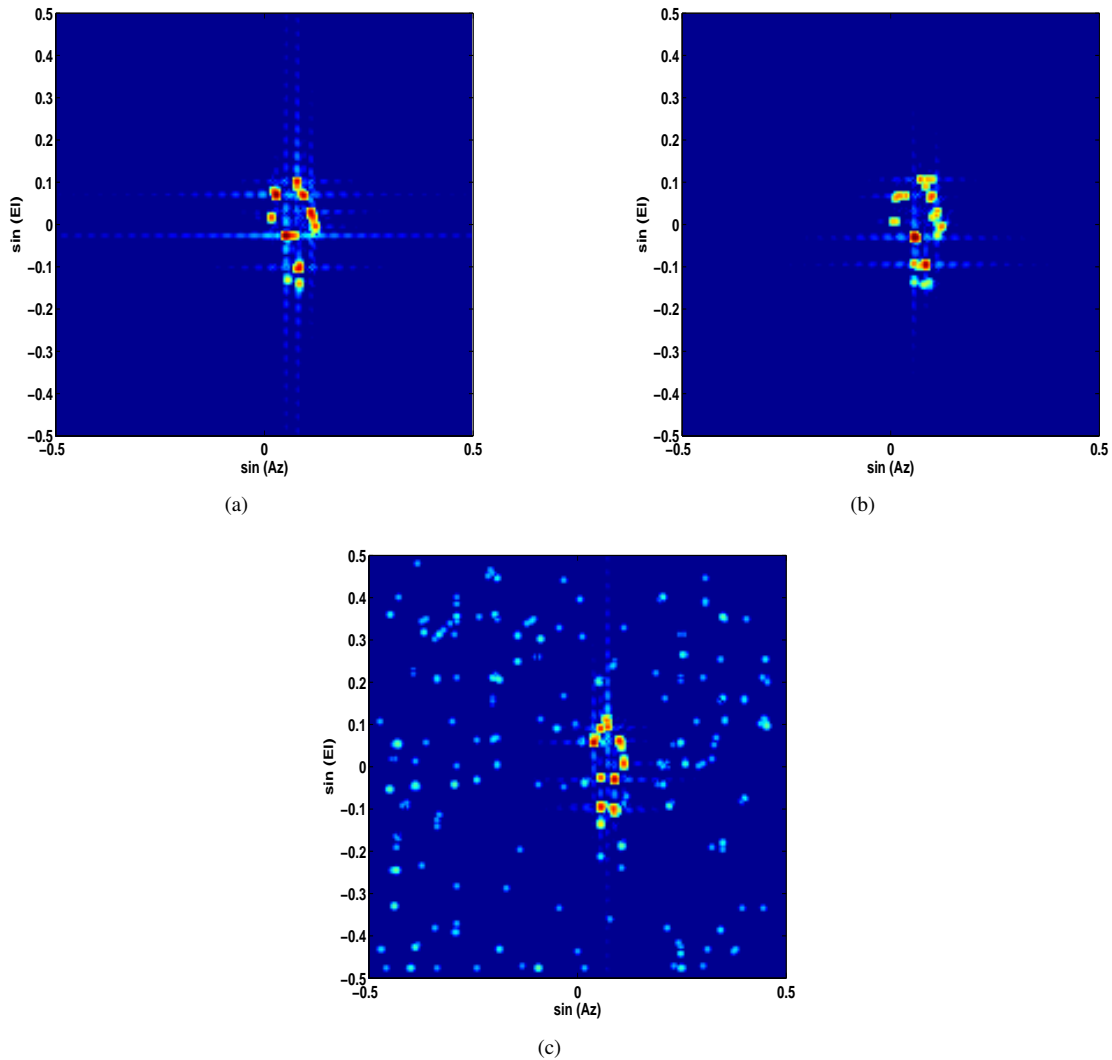


Fig. 6. Frontal radar image of a human captured by combined Doppler processing and array processing with compressed sensing using (a) 50%, (b) 10% of the number of sensors in a $[20 \times 20]$ array configuration operating at 7.5GHz. The image in (c) is generated with 25% of the number of sensors in the same radar with an SNR of 10dB.

REFERENCES

- [1] S. Nag, M. A. Barnes, T. Payment, and G. Holladay, "Ultrawideband through-wall radar for detecting the motion of people in real time," in *AeroSense 2002*. International Society for Optics and Photonics, 2002, pp. 48–57.
- [2] A. Yarovoy, L. Ligthart, J. Matuzas, and B. Levitas, "Uwb radar for human being detection," *Aerospace and Electronic Systems Magazine*, *IEEE*, vol. 21, no. 3, pp. 10–14, 2006.
- [3] S. S. Ram, Y. Li, A. Lin, and H. Ling, "Doppler-based detection and tracking of humans in indoor environments," *Journal of the Franklin Institute*, vol. 345, no. 6, pp. 679–699, 2008.
- [4] J. Sachs, M. Aftanas, S. Crabbe, M. Drutarovsky, R. Klukas, D. Kocur, T. Nguyen, P. Peyerl, J. Rovnakova, and E. Zaikov, "Detection and tracking of moving or trapped people hidden by obstacles using ultrawideband pseudo-noise radar," in *Radar Conference, 2008. EuRAD 2008. European*. IEEE, 2008, pp. 408–411.
- [5] N. Maaref, P. Millot, C. Pichot, and O. Picon, "A study of uwb fm-cw radar for the detection of human beings in motion inside a building," *Geoscience and Remote Sensing, IEEE Transactions on*, vol. 47, no. 5, pp. 1297–1300, 2009.
- [6] V. C. Chen, F. Li, S.-S. Ho, and H. Wechsler, "Micro-doppler effect in radar: phenomenon, model, and simulation study," *Aerospace and Electronic Systems, IEEE Transactions on*, vol. 42, no. 1, pp. 2–21, 2006.
- [7] G. E. Smith, K. Woodbridge, and C. Baker, "Template based micro-doppler signature classification," in *High Resolution Imaging and Target Classification, 2006. The Institution of Engineering and Technology Seminar on*. IET, 2006, pp. 127–144.
- [8] I. Bilik, J. Tabrikian, and A. Cohen, "Gmm-based target classification for ground surveillance doppler radar," *Aerospace and Electronic Systems, IEEE Transactions on*, vol. 42, no. 1, pp. 267–278, 2006.
- [9] T. Thayaparan, S. Abrol, E. Riseborough, L. Stankovic, D. Lamothe, and G. Duff, "Analysis of radar micro-doppler signatures from experimental helicopter and human data," *IET Radar, Sonar & Navigation*, vol. 1, no. 4, pp. 289–299, 2007.
- [10] Y. Kim and H. Ling, "Human activity classification based on micro-doppler signatures using a support vector machine," *Geoscience and Remote Sensing, IEEE Transactions on*, vol. 47, no. 5, pp. 1328–1337, 2009.
- [11] G. E. Smith and B. G. Mobasseri, "Robust through-the-wall radar image classification using a target-model alignment procedure," *Image Processing, IEEE Transactions on*, vol. 21, no. 2, pp. 754–767, 2012.
- [12] J. Bryan, J. Kwon, N. Lee, and Y. Kim, "Application of ultra-wide band radar for classification of human activities," *IET Radar, Sonar & Navigation*, vol. 6, no. 3, pp. 172–179, 2012.
- [13] D. R. Wehner, "High resolution radar," *Norwood, MA, Artech House, Inc., 1987, 484 p.*, vol. 1, 1987.
- [14] S. S. Ram, C. Christianson, Y. Kim, and H. Ling, "Simulation and analysis of human micro-dopplers in through-wall environments," *Geoscience*

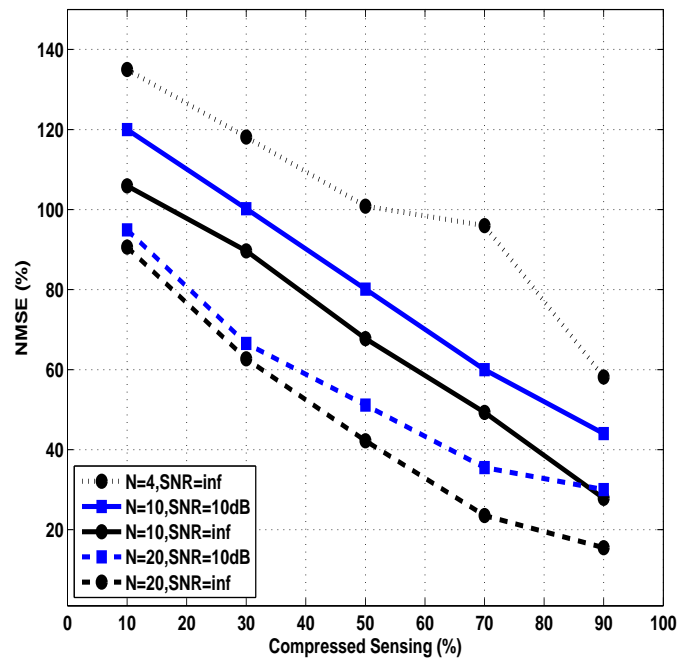


Fig. 7. Normalized mean square error of image reconstruction as a function of compression of an $[N \times N]$ array with SNR level specified as (a) $N = 5, SNR = \infty$, (b) $N = 10, SNR = 10dB$, (c) $N = 10, SNR = \infty$, (d) $N = 20, SNR = 10dB$ and (e) $N = 20, SNR = \infty$. Image reconstruction is through combined Doppler processing and compressed sensing based array processing.

- and Remote Sensing, *IEEE Transactions on*, vol. 48, no. 4, pp. 2015–2023, 2010.
- [15] A. Lin and H. Ling, “Frontal imaging of human using three-element doppler and direction-of-arrival radar,” *Electronics Letters*, vol. 42, no. 11, pp. 660–661, 2006.
- [16] D. L. Donoho, “For most large underdetermined systems of linear equations the minimal 1-norm solution is also the sparsest solution,” *Communications on pure and applied mathematics*, vol. 59, no. 6, pp. 797–829, 2006.
- [17] —, “Compressed sensing,” *Information Theory, IEEE Transactions on*, vol. 52, no. 4, pp. 1289–1306, 2006.
- [18] U. Gamper, P. Boesiger, and S. Kozierke, “Compressed sensing in dynamic mri,” *Magnetic Resonance in Medicine*, vol. 59, no. 2, pp. 365–373, 2008.
- [19] L. Chen, M. C. Schabel, and E. V. DiBella, “Reconstruction of dynamic contrast enhanced magnetic resonance imaging of the breast with temporal constraints,” *Magnetic resonance imaging*, vol. 28, no. 5, pp. 637–645, 2010.
- [20] R. Baraniuk and P. Steeghs, “Compressive radar imaging,” in *Radar Conference, 2007 IEEE*. IEEE, 2007, pp. 128–133.
- [21] M. Herman and T. Strohmer, “Compressed sensing radar,” in *Radar Conference, 2008. RADAR’08. IEEE*. IEEE, 2008, pp. 1–6.
- [22] Y.-S. Yoon and M. G. Amin, “Compressed sensing technique for high-resolution radar imaging,” in *SPIE Defense and Security Symposium*. International Society for Optics and Photonics, 2008, pp. 69 681A–69 681A.
- [23] M. A. Herman and T. Strohmer, “High-resolution radar via compressed sensing,” *Signal Processing, IEEE Transactions on*, vol. 57, no. 6, pp. 2275–2284, 2009.
- [24] L. C. Potter, E. Ertin, J. T. Parker, and M. Cetin, “Sparsity and compressed sensing in radar imaging,” *Proceedings of the IEEE*, vol. 98, no. 6, pp. 1006–1020, 2010.
- [25] V. M. Patel, G. R. Easley, D. M. Healy Jr, and R. Chellappa, “Compressed synthetic aperture radar,” *Selected Topics in Signal Processing, IEEE Journal of*, vol. 4, no. 2, pp. 244–254, 2010.
- [26] Q. Huang, L. Qu, B. Wu, and G. Fang, “Uwb through-wall imaging based on compressive sensing,” *Geoscience and Remote Sensing, IEEE Transactions on*, vol. 48, no. 3, pp. 1408–1415, 2010.
- [27] S.-J. Wei, X.-L. Zhang, J. Shi, and G. Xiang, “Sparse reconstruction for sar imaging based on compressed sensing,” *Progress In Electromagnetics Research*, vol. 109, pp. 63–81, 2010.
- [28] A. C. Fannjiang, T. Strohmer, and P. Yan, “Compressed remote sensing of sparse objects,” *SIAM Journal on Imaging Sciences*, vol. 3, no. 3, pp. 595–618, 2010.
- [29] S.-J. Wei, X.-L. Zhang, and J. Shi, “Linear array sar imaging via compressed sensing,” *Progress In Electromagnetics Research*, vol. 117, 2011.
- [30] E. Aguilera, M. Nannini, and A. Reigber, “Wavelet-based compressed sensing for sar tomography of forested areas,” in *Synthetic Aperture Radar, 2012. EUSAR. 9th European Conference on*. VDE, 2012, pp. 259–262.
- [31] —, “Multisignal compressed sensing for polarimetric sar tomography,” *Geoscience and Remote Sensing Letters, IEEE*, vol. 9, no. 5, pp. 871–875, 2012.
- [32] —, “A data-adaptive compressed sensing approach to polarimetric sar tomography of forested areas,” *Geoscience and Remote Sensing Letters, IEEE*, vol. 10, no. 3, pp. 543–547, 2013.
- [33] J. Fang, Z. Xu, B. Zhang, W. Hong, and Y. Wu, “Fast compressed sensing sar imaging based on approximated observation,” *Selected Topics in Applied Earth Observations and Remote Sensing, IEEE Journal of*, 2013.
- [34] Y.-S. Yoon and M. G. Amin, “Imaging of behind the wall targets using wideband beamforming with compressive sensing,” in *Statistical Signal Processing, 2009. SSP’09. IEEE/SP 15th Workshop on*. IEEE, 2009, pp. 93–96.
- [35] Y. Yu, A. P. Petropulu, and H. V. Poor, “Mimo radar using compressive sampling,” *Selected Topics in Signal Processing, IEEE Journal of*, vol. 4, no. 1, pp. 146–163, 2010.
- [36] S. Gogineni and A. Nehorai, “Target estimation using sparse modeling for distributed mimo radar,” *Signal Processing, IEEE Transactions on*, vol. 59, no. 11, pp. 5315–5325, 2011.
- [37] A. Majumdar and S. S. Ram, “Two dimensional array processing with compressed sensing,” in *Radar Conference, 2014. RADAR’14. IEEE*. IEEE, 2014, pp. 1–4.
- [38] I. Selesnick. (2009) About: Sparse signal restoration. [Online]. Available: http://cnx.org/content/m32168/1.3/content_info
- [39] V. C. Chen and H. Ling, *Time-frequency transforms for radar imaging and signal analysis*. Artech House, 2002.